ISSN 1063-780X, Plasma Physics Reports, 2024, Vol. 50, No. 1, pp. 1–11. © The Author(s), 2024. This article is an open access publication.

MAGNETIC TRAPS

Investigation of Plasma Flow Velocity in the Helical Magnetic Open Trap SMOLA

A. A. Inzhevatkina[a,*], I. A. Ivanov[a], V. V. Postupaev[a], A. V. Sudnikov[a], M. S. Tolkachev[a], and V. O. Ustyuzhanin[b]

[a] *Budker Institute of Nuclear Physics, Siberian Branch, Russian Academy of Sciences, Novosibirsk, 630090 Russia*

[b] *Novosibirsk State University, Novosibirsk, 630090 Russia*

**e-mail: a.a.inzhevatkina@inp.nsk.su*

Received July 24, 2023; revised October 20, 2023; accepted November 1, 2023

Abstract—The physics of confinement of plasma rotating in the magnetic field with linear helical symmetry is studied at the SMOLA open trap at Budker Institute of Nuclear Physics of the Siberian Branch of the Russian Academy of Sciences. The factor characterizing the quality of plasma confinement in the system is its flow velocity. The paper describes the diagnostics applied, which is based on the Mach probe used under the conditions of nonmagnetized plasma; this diagnostics made it possible to determine the longitudinal flow velocity in the experiments. In different operating regimes of the device, the measured longitudinal flow velocity was $(0.5–5) \times 10^6$ cm/s. It is discussed how the velocity depends on the magnetic field corrugation. The reverse flow of trapped particles returning to the confinement zone was detected.

Key words: magnetic confinement, open trap, helical confinement, SMOLA, Mach probe, flow velocity

DOI: 10.1134/S1063780X23602031

1. INTRODUCTION

The development of studies of the physics of plasma confinement in open magnetic traps has a long history [1]. Advances in the physics and technology of plasma confinement in open magnetic systems [2] make it possible to design new-generation open traps [3–5], which are of interest not only in terms of studying the magnetic confinement or different materials and structures, but also in terms of using such device as neutron sources [6] or pure fusion reactors. Achievements based on the results of experimental studies at the GOL-3 [7] and GDT [8] device made it possible to design the new-generation trap GDMT (Gas Dynamic Multiple-Mirror Trap) at Budker Institute of Nuclear Physics of the Siberian Branch of the Russian Academy of Sciences [9]. The physical program of studies provides for the integration of several known methods for improving longitudinal plasma confinement in one experimental device, in order to demonstrate the possibility of obtaining plasma with parameters interesting for fusion applications in open trap. Some of the physical principles and techniques are currently undergoing experimental verification at the GOL-NB [10], CAT [11], and SMOLA [12] small devices. Each of these systems is a prototype of the GDMT functional modules.

The SMOLA facility is the first system using linear multiple-mirror sections with helical symmetry of the magnetic field. Such a magnetic system resembles the straightened magnetic system of a classical stellarator. Unlike the stellarator, the helical system is optimized to obtain the maximum field corrugation, which can be achieved using one pair of helical current-carrying elements [13]. Quite the contrary, the rotational transformation is not one of the key parameters for the system optimization and is limited only by the MHD instability. If in the helical trap, plasma rotates around the axis, for example, due to $E \times B$ drift, the magnetic mirrors moving along the axis occur in the rotating plasma reference frame [14]. Such motion is able to transfer the longitudinal momentum from the magnetic field coils to the plasma flow. Due to plasma viscosity or collisions with locally trapped particles, the plasma in general will acquire the longitudinal momentum component, which will result in the occurrence of a force that can be used for slowing down or accelerating plasma flows.

In the system with helical magnetic mirrors, plasma deceleration by the external force provides for better longitudinal confinement, which makes it possible to obtain higher plasma parameters in the trap under the same technical limitations on the parameters of the magnetic system and plasma heating systems. The momentum transfer between the plasma and magnetic mirror is accompanied by the occurrence of radial drifts and currents arising from the axial

symmetry breaking. In theory, such radial drifts result in plasma pinching at the system axis, i.e., in the process counteracting radial diffusion [15, 16]. In previous experiments at the SMOLA device, it was observed that the predicted effects are indeed observed; improved longitudinal plasma confinement in the trap with helical magnetic field symmetry was demonstrated at moderate collisionality when the mean free path is comparable with the period of helical field corrugation [17–19]. For reactor-grade systems, the weakly collisional flow regime is of more interest. Efficient momentum transfer from the plasma flow through the population of locally trapped particles to the magnetic field can also occur in this case if the difference between the flow velocities of these particle populations is considerably high. Then the appearance of two-stream instability will make such friction efficient even in weakly collisional plasma.

In the presence of longitudinal velocity of magnetic perturbations, the matter flow in the multiple-mirror field can be written as follows:

$$\rho V_{\parallel} = D\frac{\partial \rho}{\partial z} + \varkappa \rho V_z,$$

$$D \sim \lambda V_{Ti}, \frac{\partial \rho}{\partial z} \sim \frac{\rho}{L}, V_z \approx c\frac{hE_r}{2\pi r B_z},$$

where ρ is the mass density, $V_{||}$ is the longitudinal flow velocity, D is the diffusion coefficient, $\varkappa$ is the fraction of trapped particles, V_z is the longitudinal velocity of magnetic perturbations in the plasma reference frame, λ is the mean free path, V_{Ti} is the thermal velocity of ions, and h is the length of one section (cell) of multiple-mirror field. In this expression, the first summand describes the diffusion broadening of plasma in the multiple-mirror magnetic field [20], while the second summand defines the additional flow associated with the motion of local potential wells containing trapped particles. In the multiple-mirror trap, efficient plasma confinement is achieved at the mean free path equal to the length of one cell. In weakly collisional plasma, this is fulfilled in the presence of anomalous scattering [21]. Thus, under assumption of $\lambda \approx h$, the diffusion coefficient is $D = hV_{Ti}$. When the V_z velocity is negative (i.e., directed counter to the plasma flow), at any point of the plasma column, the local flux can be reduced as compared to that in the multiple-mirror configuration. We would like to note that the longitudinal component of the $[E \times B]$ drift velocity $V_{[E\times B]z}$ is negligibly small as compared to the V_z velocity, since

$$\frac{V_{[E\times B]z}}{V_z} = \frac{B_\theta}{B_z}\frac{2\pi r}{h} < \frac{(2\pi r)^2}{Lh} \sim \frac{h}{L} \sim \frac{1}{N} \ll 1,$$

where h is the length of a single cell of the multiple-mirror field, L is the trap length, and N is the number of corrugation periods, while the design feature of the device is the fulfilment of relation $2\pi r \sim h$ [13]. Hence, the local plasma velocity can be expressed as follows:

$$V_{\parallel} \sim \frac{h}{L}V_{Ti} - \varkappa c\frac{hE_r}{2\pi r B_z},$$

where $V_{||}$ is the longitudinal flow velocity, L is the trap length, E_r is the radial electric field, and B_z is the magnetic field. We note that that in the second summand, when approaching the axis, there simultaneously occurs a faster decrease of the corrugation depth along the force line, due to which the fraction of trapped particles decreases.

Thus, the local flow velocity can become negative, i.e., in some regions of the plasma column, the flow can be directed from the trap outlet towards the confinement zone. Such a situation does not contradict the law of conservation of matter, since the trapping of particles in potential wells and their subsequent motion together with the magnetic perturbations can occur in different spatial regions. In accordance with the theory of radial and longitudinal transport of particles in the helical magnetic field [16], at the negative potential at the plasma axis, the transport of ions in the course of their scattering through the loss cone boundary can result in similar effect. Thus, in open trap with the helical magnetic field, the plasma flow velocity is an indicator of the quality confinement.

In the helical magnetic field, the efficiency of longitudinal plasma confinement is affected by the angular rotation velocity. This velocity is determined by the radial electric field, the distribution of which is determined by the potentials of the plasma source, radial segmental endplate and limiter system. The longitudinal velocity of the plasma flow, flowing out and returning back to the confinement zone, indicates how strongly the helical field affects the number of trapped particles returned back to the confinement zone.

In this work, we experimentally study the dependences of the longitudinal velocity of motion in the transport section of the SMOLA device on the magnitude of the magnetic field corrugation. Two diagnostics were used to measure the longitudinal velocity at different points inside the trap: the high spatial resolution Doppler spectroscopy [22] and the Mach probes.

Section 2 describes the SMOLA open helical trap. In Section 3, the design of the Mach probe and the method for determining the longitudinal velocity are described. In Section 4, the experimental results are presented obtained using both the probe installed perpendicularly to the plasma flow and the rotating probe. The occurrence of reverse flow of trapped particles returning back to the confinement zone was demonstrated, and some estimates of the fraction of these particles were obtained.

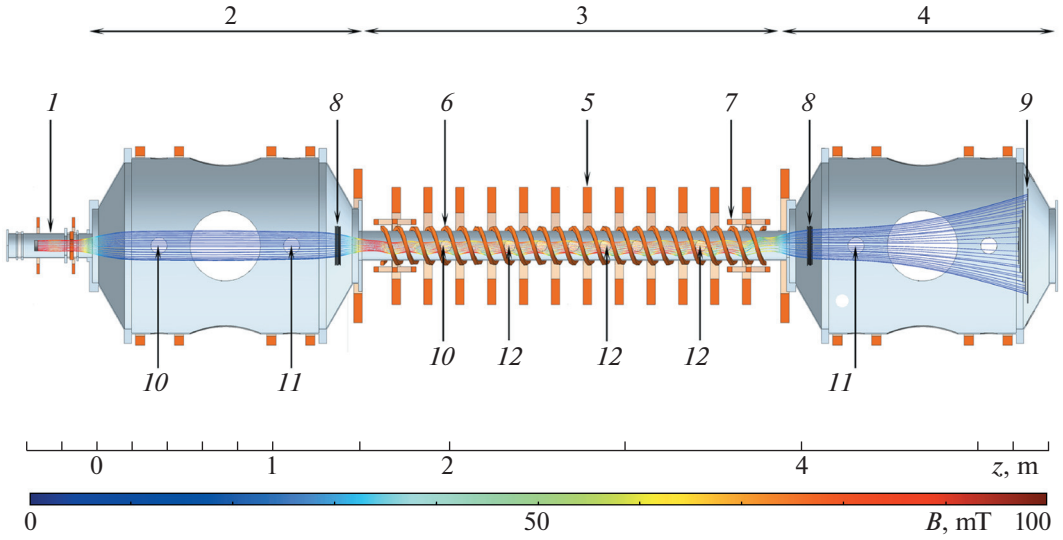

Fig. 1. Schematic of the SMOLA device and diagnostics used: (*1*) plasma source, (*2*) inlet expander (confinement zone), (*3*) transport section, (*4*) outlet expander, (*5*) straight solenoid, (*6*) helical coils, (*7*) coils for correcting plasma jet position, (*8*) limiter, (*9*) endplate, (*10*) probe assembly: double probe and two emission probes, (*11*) Doppler spectrometer, and (*12*) probe assembly: Mach probe and two emission probes. Individual coils are shown as rectangles. Thin lines near axis show magnetic surface touching the limiters.

2. EXPERIMENTAL

Figure 1 shows the schematic of the SMOLA device, which includes the plasma source based on heated LaB_6 cathode [23], confinement zone (inlet expander), multiple-mirror helical section, and outlet expander of the plasma flow. In further consideration, the outlet aperture of the plasma source is taken as the origin for the Z longitudinal coordinate. The magnetic system consists of the plasma gun coils, coils of the inlet and outlet expanders, central solenoid with the helical field coil, and coils correcting the plasma jet position. The straight and helical magnetic field components are set independently of each other.

The outlet expander is equipped with the radial segmental endplate consisting of five concentric rings, the potential of each is applied independently. The voltage between each pair of neighboring plates of the endplate is $U = 50$ V. At the inlet and outlet of the transport section, the sectionalized limiters are installed that provide for limitation of the plasma jet and the possibility of introducing potential into the plasma. The voltage in the range from −150 to 150 V with respect to the device body can be supplied to the inlet limiter.

Ranges of basic parameters of the SMOLA device are given in Table 1.

The magnetic field configuration in this experimental series is shown in Fig. 2 at the guiding magnetic field in the transport section of 70 mT in the case of straight field ($R = 1$). Hereinafter, R is the ratio of the maximum and minimum magnetic fields on a given force line inside the transport section, averaged over the plasma cross-section. Obviously, the local mirror ratio is maximum at the peripheral force lines and decreases to unity at the magnetic axis. The magnetic field is changed synchronously in the plasma source region, confinement zone, transport section, and outlet expander so that the configuration of the force lines remains unchanged.

Experimental campaigns were carried out in two configurations, which differ in the magnetic fields in the regions of anode coil, and inlet and outlet limiters. Such variations affect the radial distributions of the electric field (Fig. 3) and plasma density (Fig. 4), and hence, the angular velocity in the transport section. In Section 4.1, we present the results obtained at the reduced field in the regions near the anode of plasma source and limiters (red dashed line in Fig. 2). In this magnetic configuration, the field line starting at the anode edge touches the limiter. Hereafter in the text, this configuration will be referred to as the "wide jet

Table 1. Basic parameters of the SMOLA facility [13]

Parameter	Value
Ion density of plasma n_i, 10^{18} m^{-3}	0.3–6
Electron temperature T_e, eV	5–35
Ion temperature T_i, eV	2–7
Plasma radius a, cm	5–10
Discharge duration $t_{discharge}$, s	0.15–1.5
Magnetic field B_z, mT	50–150
Radial electric field E_r, V/cm	10–35

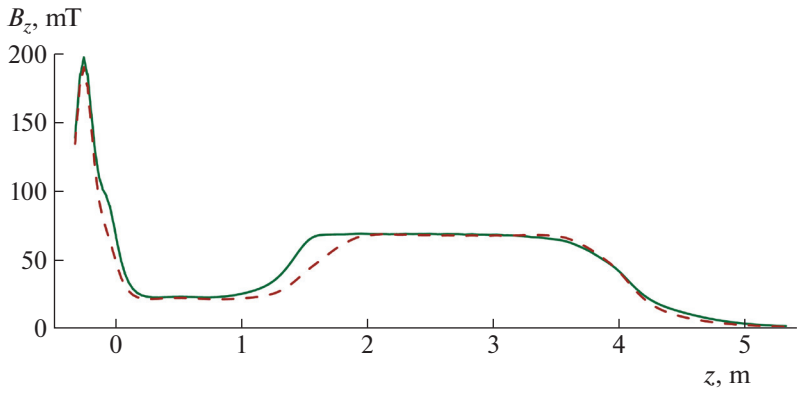

Fig. 2. Magnetic field configurations at guiding magnetic field of 70 mT in solenoid and straight field: red dashed and green solid lines correspond to "wide" and "narrow" jet regimes, respectively.

regime". In Subsection 4.2 we present the results obtained at the increased field in the anode coil region of the plasma source and at the limiters (green solid line in Fig. 2). The field line starting at the anode edge does not touch the limiter, the gap between them being $dr \sim 5$ mm. In this case, the electrical contact between the plasma and the limiter is weakened. Hereafter in the text, this configuration will be referred to as "narrow jet regime". In all cases, the guiding magnetic field in the transport section is 70 mT.

For observing the plasma emission in the outlet expander, the spectrometer with spatial resolution based on the MDR-23 monochromator [22] was installed either at $Z = 4.34$ m (Fig. 1) at an angle of 90º to the axis in order to determine only the azimuthal velocity, or at $Z = 5.3$ m at an angle of 30º to the axis (Fig. 1) in order to observe the Doppler shift of the H_α emission line, corresponding to the velocity defined as follows:

$$V = V_\varphi \sin\alpha + V_\parallel \cos\alpha,$$

where V is the velocity recorded by the spectrometer, V_φ is the azimuthal velocity, and $V_\parallel$ is the longitudinal velocity of plasma motion.

3. MACH PROBE DESIGN AND CHARACTERISTIC FEATURES

The Mach probe is a pair of double Langmuir probes closely positioned and separated from each other by insulating quartz partition. If there occurs some flow velocity, i.e., asymmetry of the plasma distribution function at the observation point, the signals of these probes will differ. The velocity and ratio of ion

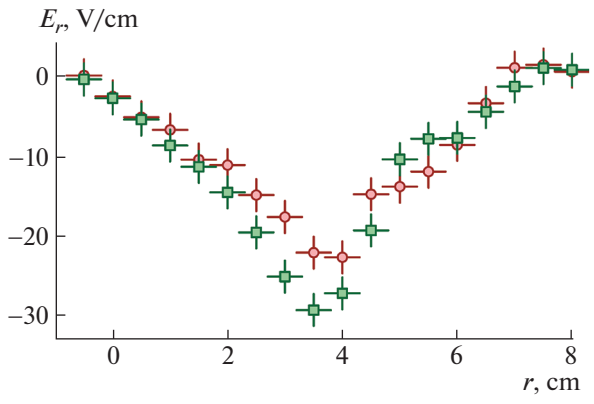

Fig. 3. Radial distributions of electric field at $Z = 2.04$ m in different magnetic field configurations: red circles and green squares correspond to "wide" and "narrow" jet regimes, respectively.

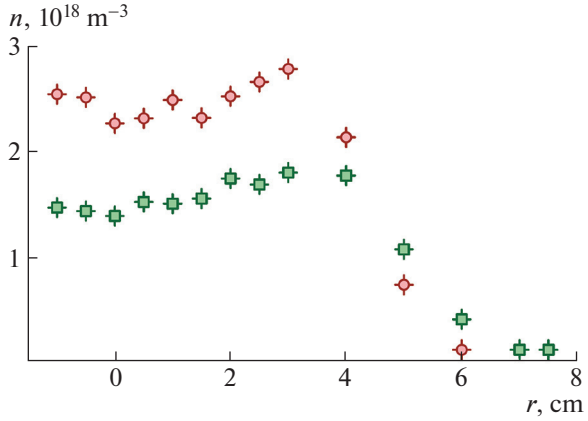

Fig. 4. Plasma density distributions at $Z = 2.04$ m in different magnetic field configurations: red circles and green squares correspond to "wide" and "narrow" jet regimes, respectively.

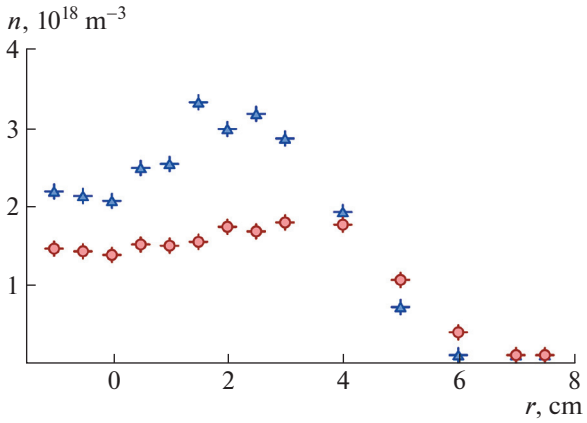

Fig. 5. Plasma density distributions at $Z = 2.04$ m in "narrow jet regime": red circles and blue triangles correspond to straight and helical fields, respectively.

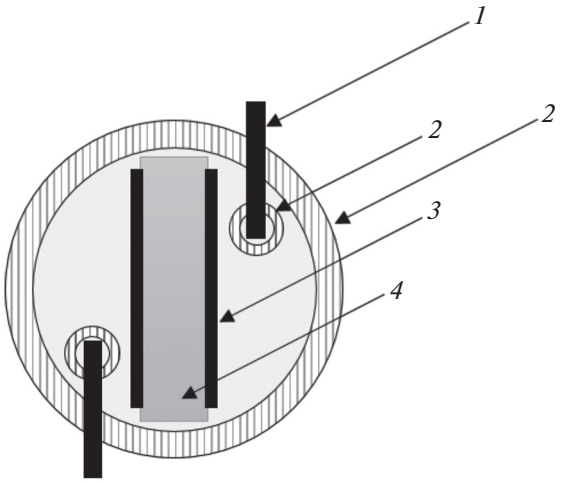

Fig. 6. Schematic of Mach probe at the SMOLA device: (*1*) tungsten wire, (*2*) ceramic capillary, (*3*) sputtered molybdenum electrode, and (*4*) quartz plate.

saturation currents from the "upstream" and "downstream" sides are related to each other as follows [24]:

$$J = \frac{I_{\text{up}}}{I_{\text{down}}} = \exp(kM),$$

where I_{up} is the saturation current of ions moving from the plasma gun side, which is recorded by the "upstream" side of the Mach probe, I_{down} is the saturation current of ions moving from the side of endplate, which is recorded by the "downstream" side of the Mach probe, the Mach number is $M = V_{\|}/C_s$, $C_s = \sqrt{T_e/m_i}$, k is the coefficient determined by the chosen model of system description, and J is the ratio of saturation currents of probes located at different sides of the partition. Hence, the flow velocity can be written as follows:

$$V_{\|} = \frac{\ln\left(\frac{I_{\text{up}}}{I_{\text{down}}}\right)}{k} c_s.$$

The interpretation of the results is complicated by the necessity of taking into account the effect of the magnetic field on the procedure of collecting ions by the electrodes. In the case under consideration, it is reasonable to consider the model of nonmagnetized plasma, since in the SMOLA device, the ion Larmor radius, $\rho_i = 0.6$–1.8 cm, exceeds the characteristic probe dimensions. As a simple model, we chose one of the models proposed in [25], obtained analytically in the approximation $T_i \ll T_e$, which is true for the plasma parameters at the SMOLA device. The model coefficient k, which interrelates the asymmetry of the probe signals and the Mach number, can be defined as follows:

$$k = 4\sqrt{\frac{T_i}{T_e}}.$$

This model describes one-dimensional cylindrically symmetric system under the assumption that the potential drops in the "upstream" and "downstream" electrodes vary due to the presence of drift velocity.

The electron temperature and plasma density are determined from the current–voltage characteristics (CVC) of the double Langmuir probe [23]. The radial electric field is measured directly using two emission probes installed along the radius and spaced by 1 cm [19]. The ion temperature is determined from data on the Doppler broadening of the H_α spectral line using the optical diagnostics based on the spectrometer with high spatial resolution. This technique allow us to determine the radial distribution of ion temperature in each plasma discharge. The spectrometers were installed at $Z = 1.15$ and 4.34 m.

In the case of nonmagnetized plasma, the design of Mach probes is more complicated in order to correctly determine the flow of ions flying strictly from the "upstream" or "downstream" sides. In order to avoid problems associated with the interpretation of data on the ion saturation currents obtained, the following design of the Mach probe was proposed, schematically represented in Fig. 6.

The Mach probe is designed in the form of two asymmetrical double probes, in which the ion collecting electrodes are molybdenum layers with thickness of ≈ 1 μm, which are sputtered on quartz plate, and the electron collecting electrodes are tungsten wires 200 μm in diameter placed in separate ceramic capillary tubes. The quartz plate is used as an insulating partition, on which the electrodes are sputtered on both sides. The flat design of the probe prevents from registrating ions flying from the back side of the plate, minimizing misinterpretation of the results.

When applying the Mach probes in open magnetic systems, another problem is that the probe creates the low-density geometric shadow downstream relative to the partition. This affects the current density recorded by the probe in the collisional plasma. If the ion mean free path is shorter than the probe shadow length, the use of standard formulas provides for wrong Mach numbers. In [26], it was considered how the probe shadow can affect the recorded plasma density in open systems. We have made similar estimates of diffusion and size of the shadow formed by the probe

The length of the geometric shadow of the probe can be estimated as follows:

$$L_g = \frac{d^2 V_d}{D_\perp} \sim 5\text{cm},$$

where V_d is the drift velocity of plasma ions, d is the probe size, and $D_\perp$ is the transverse diffusion coefficient. The length of the depleted-density region in the plasma, occurring due to the effect of the probe as a physical obstacle, does not exceed the period of the magnetic field corrugation, so, under conditions considered, we can use the Mach probe and the above model.

Relative calibration of the two Mach probe channels was performed by means of rotating it by 180°, in order to find the ratio of areas of the collecting surfaces. As an independent calibration, in one longitudinal cross-section of the transport section, we performed measurements of the azimuthal plasma velocity using the Mach probe rotated by 90° and the electric field measurements using the emission probes. The velocities measured using the Mach probe and calculated from the radial electric field distribution coincide and reach the ion-acoustic velocity at the plasma periphery (in the region with the maximum E_r field). This does not contradict the previously obtained data [22].

The Mach probe mounted on the rotary feedthrough providing for the probe rotation with a step of 15° allow us to determine not only the absolute value of plasma velocity, but also the angle between the velocity direction and the guiding magnetic field. The flow velocity as a function of the probe rotation angle looks as follows:

$$V = V_\parallel \cos\theta + V_\varphi \sin\theta = V_0 \cos(\theta + \varphi_0),$$

where $V_{||}$ is the flow velocity, V_φ is the azimuthal velocity, and φ_0 is the angle between the direction of plasma flow velocity and the guiding magnetic field.

The positioning system provides for probe rotation in 15° increments and probe radial motion in the range from 0 to 4 cm.

The velocity absolute value can be also determined using the stationary Mach probe measuring only the longitudinal velocity and two emission probes spaced by 1 cm and measuring the radial electric field. Then the velocity absolute value and its angle with respect to the guiding magnetic field can be determined using the following expressions:

$$V = \sqrt{V_\parallel^2 + (V_\varphi)^2} = \sqrt{V_\parallel^2 + \left(c\frac{E_r}{B}\right)^2},$$

$$\theta = \operatorname{arccot}\left(\frac{V_\parallel}{V_\varphi}\right).$$

Thus, using two independent ways of measuring the parameters, it is possible to compare the data obtained and determine whether each of the diagnostics is operating correctly.

In the model of plasma transport in the helical field [14], it is assumed that in the helical field, there occurs the reverse particle flow due to the plasma pinching towards the axis of the plasma column, an increase in the radial electric field, and the development of two-stream instability resulting in the motion of a population of trapped particles with supersonic speed towards the confinement zone.

We consider the following model of particle motion. In the multiple-mirror trap with moving mirrors, three populations of particles can be distinguished: trapped particles and transiting ones with positive and negative velocity projections equal to V_{Ti}. Taking into account the densities and velocities of each of the populations, we can determine the average longitudinal velocity of motion as follows:

$$\langle V_\parallel \rangle = \frac{n_1 V_{T_i} - n_3 V_{T_i} - n_2 V_z}{n},$$

where $V_{||}$ is the longitudinal velocity of motion, V_{Ti} is the thermal velocity, V_z is the velocity of moving magnetic perturbation, n is the total density, n_1 is the density of transiting particles moving towards the outlet expander, n_3 is the density of transiting particles returning to the confinement zone, and n_2 is the density of trapped particles moving together with the magnetic perturbations.

Taking into account that in the straight field ($R = 1$), there is no reverse flow of trapped particles moving together with the magnetic perturbations, we can compose the following set of equations:

$$\begin{cases} \langle V_{\parallel h} \rangle = \dfrac{n_{1h} V_{T_{ih}} - n_{3h} V_{T_{ih}} - n_2 V_z}{n_h}, \quad \text{at } R > 1, \\ \langle V_{\parallel s} \rangle = \dfrac{n_{1s} V_{T_i s} - n_{3s} V_{T_{is}}}{n_s} \quad \text{at } R = 1, \\ n = n_1 + n_2 + n_3, \\ n_2 = \varkappa n, \end{cases}$$

where the h and s indices corresponds to the helical and straight fields, respectively, and $\varkappa$ is the fraction of trapped particles moving due to the motion of mag-

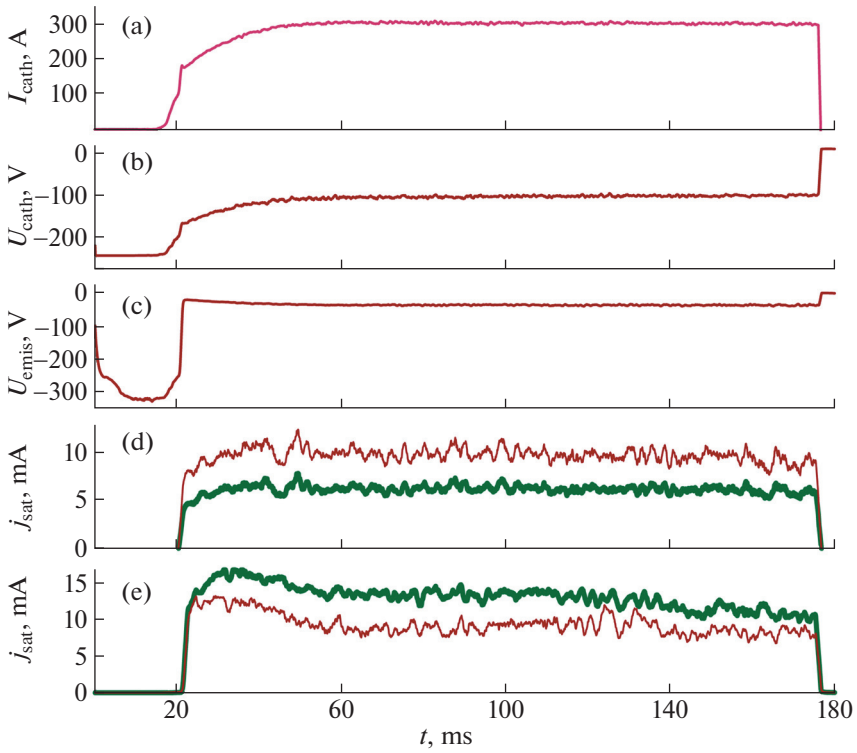

Fig. 7. Typical oscillograms of basic signals: (a) plasma current, (b) voltage supplied between anode and cathode of plasma source, (c) emission probe potential, and (d) and (e) ion saturation currents of probes located at "upstream" (*up*, thin red line) and "downstream" (*down*, thick green line) sides in straight and helical magnetic fields, respectively.

netic perturbations in the rotating plasma reference frame.

Solving set of equation with allowance for relation $V_{Tih} \approx V_{Tis}$, we obtain the following correlations for the densities of particles moving in forward and backward directions:

$$\frac{n_1}{n_3} = \frac{V_{T_i} + V_\parallel}{V_{T_i} - V_\parallel},$$

as well as for the fraction of trapped particles:

$$\varkappa = \frac{n_2}{n} = \frac{V_{\parallel_s} - V_{\parallel_h}}{V_{\parallel_s} + V_z}.$$

4. RESULTS AND DISCUSSION

4.1. Experimental Scenario

In the series of experiments described, we studied the dependence of the longitudinal velocity of motion on the average depth of magnetic field corrugation determined by the ratio of currents in the solenoidal and helical windings of the transport section. The Mach probes were installed in the transport section of the SMOLA device at the coordinates $Z = 2.4$, 2.94, and 3.48 m. The profiles of the ion saturation currents at the "upstream" and "downstream" sides were measured in 5 mm increments along the plasma radius.

Next we will discuss the experimental data obtained at the guiding magnetic field of 70 mT and the amount of gas puffed into the gas-discharge region of the plasma source of ~2×10^{20} atoms/s. Typical oscillograms of the basic signals in the described experiments are shown in Fig. 7. The ion saturation current is determined by means of averaging data over time interval from the 90th to 150th ms counted from the beginning of discharge. The RMS value of fluctuations of the measured saturation current is ~ 0.4 mA.

4.2. Comparison of Velocities Obtained Using Different Diagnostic Methods

In the "wide jet regime," the series of experiments on determining the flow velocity were carried out. The longitudinal velocities obtained using the methods of both probe measurement and Doppler spectrometry were compared. Figure 8 shows the flow velocity as a function of the Mach probe rotation angle. The velocities presented are both negative and positive. This is consistent with the fact that the "upstream" and "downstream" probe sides replace each other when the probe rotates, and the absolute values of velocity are almost the same for the strictly perpendicular probe and the probe rotated by 180°. The velocity distribution obtained corresponds to the function of the

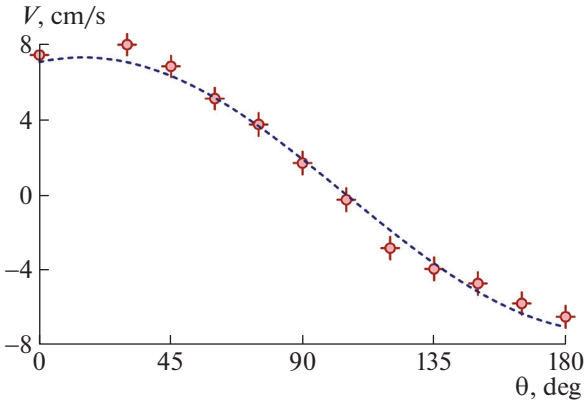

Fig. 8. Flow velocity as a function of rotation angle of Mach probe at $Z = 2.4$ m and $r = 1$ cm. Red circles correspond to results obtained experimentally, and blue dashed line shows inscribed trigonometric function.

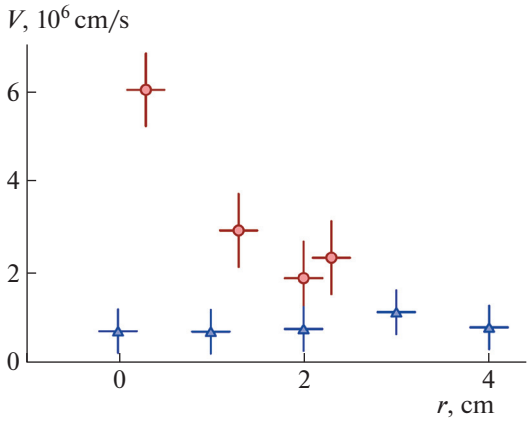

Fig. 9. Absolute values of plasma motion velocity in straight (red circles) and helical (blue triangles) magnetic fields at $Z = 2.4$ m.

form $V = V_0 \cos(\theta + \varphi_0)$, where $V_0 = (7.3 \pm 0.9) \times 10^6$ cm/s, and $\theta = 15 \pm 3°$.

Figure 9 shows the radial distributions of the absolute value of plasma velocity in the transport section in the straight ($R = 1$) and helical ($R = 1.52$) magnetic fields. In the straight magnetic field, the velocity is higher than that in the helical field throughout the plasma column. This difference increases when approaching the axis. In the "wide jet regime", no reverse flow is observed, which may be due to insufficient radial electric field, and, accordingly, radial transport. Thus, the conditions for reaching the velocity of magnetic perturbations sufficient for the occurrence of reverse flow are not satisfied. At the reduced radial electric field, the angular velocity, which is one of the basic parameters affecting the quality of confinement, decreases at the edge, which results in inefficient momentum transfer to the trapped particles from the edge to the axis of the plasma column. As a consequence, in the straight field, the plasma near the axis flows out with high velocity.

To verify the correctness of the measurement data obtained using the rotating probe ($Z = 2.4$ m), we compared the velocities and angles with respect to the guiding magnetic field with the results obtained using the probe assembly that can be displaced along the radius ($Z = 2.94$ m). At the axis of the plasma column, the radial electric field is zero. So, knowing its distribution, we can find out where is the center of the plasma jet, which makes it possible to compare the obtained velocities in the same coordinates. The radial dependences of the velocity absolute values measured in two coordinates are presented in Fig. 10. It can be seen that the velocity ranges and radial dependences coincide. The maximum longitudinal velocity of $\sim 5 \times 10^6$ cm/s is observed in the central region. The data on the longitudinal velocity obtained agree with the results obtained previously.

Figure 11 presents the results of measurements of the angle between the flow velocity and the guiding magnetic field performed in the straight magnetic field using the same probes. This angle depends on the local radial electric field causing the $E \times B$ drift of the plasma. We can see that the angle between the plasma flow velocity and the guiding magnetic field ranges from 0° to 90°. As the plasma radius increases, this angle also increases, while the flow velocity decreases. The maximum electric field is observed at the radius corresponding to the projection of the limiter. Figure 11 shows that it is the azimuthal velocity that makes the maximum contribution to the velocity absolute value at this radius.

There are two different ways of measuring the flow velocity absolute value and the angle between the velocity and guiding magnetic field: the direct measurements using the rotating Mach probe and the

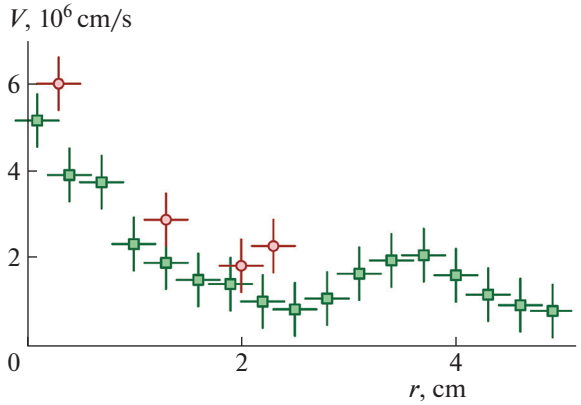

Fig. 10. Radial dependences of absolute value of plasma velocity: red circles and green squares correspond to measurements performed using rotating probe installed at $Z = 2.4$ m and probe assembly installed at $Z = 2.94$ m.

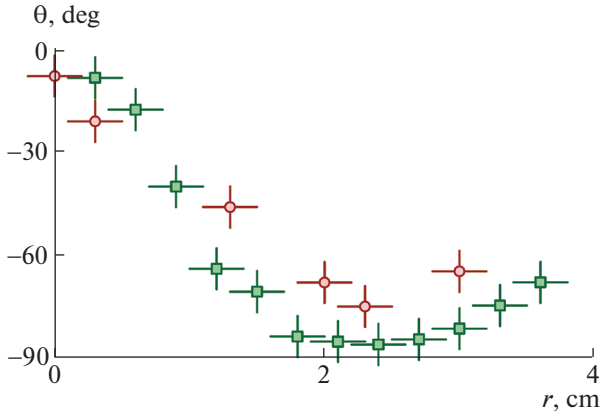

Fig. 11. Radial dependences of angle between flow velocity and guiding magnetic field: red circles and green squares correspond to measurements performed using rotating probe installed at $Z = 2.4$ m and probe assembly installed at $Z = 2.94$ m.

measurements of the radial electric field and the longitudinal velocity component. These two methods give close results, with allowance for the measurement errors and the fact that the probes are located not in the same coordinate along the facility length.

To verify the results obtained using the probe techniques, the plasma flow velocity in the outlet expander of the SMOLA device was determined using the Doppler spectrometry. For $R = 1$, we obtained the radial distribution of the azimuthal velocity in the outlet expander (Fig. 12a), which corresponds to the solid-state rotation with the angular velocity $\omega \approx 0.61 \times 10^6$ s^{-1}. Figure 12b shows the radial dependence of the plasma flow velocity in the outlet expander. The maximum longitudinal velocity of $V_\parallel \sim 4 \times 10^6$ cm/s is reached at the axis of the plasma column. This velocity agrees with the expected estimates and velocities obtained using the Mach probes, with allowance for the locations of the diagnostics in the outlet expander and transport section, respectively. This velocity distribution is characteristic of experimental campaigns carried out in the straight magnetic field in the "wide jet regime." This set of diagnostics allow us to measure the plasma flow velocities along the entire facility length during one experimental shot with the required accuracy.

4.3. Observations of Reverse Plasma Flow

Experiments on studying the effect of the helical modulation depth (corrugation) of the magnetic field in the transport section on the longitudinal velocity of plasma motion were carried out in the magnetic configuration shown in Fig. 2 in the "narrow plasma jet regime."

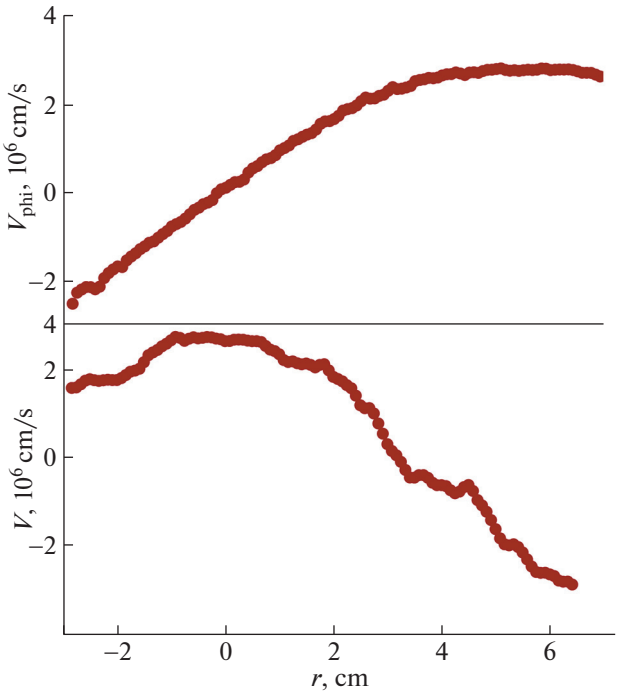

Fig. 12. (a) Radial dependence of azimuthal plasma velocity in straight field measured in outlet expander at $Z = 4.34$ m and (b) radial dependence of flow velocity in straight field measured in outlet expander at $Z = 5.3$ m.

Figure 13 shows the profiles of ion saturation currents at the "upstream" and "downstream" sides of the Mach probe measured at $Z = 2.94$ m for the cases of straight ($R = 1$) and helical ($R = 1.52$) fields in the transport section. The profiles of the ion saturation currents demonstrate that in the transport section, the maximum density was reached near the radius $r = 3$ cm, while the density at the axis of the plasma col-

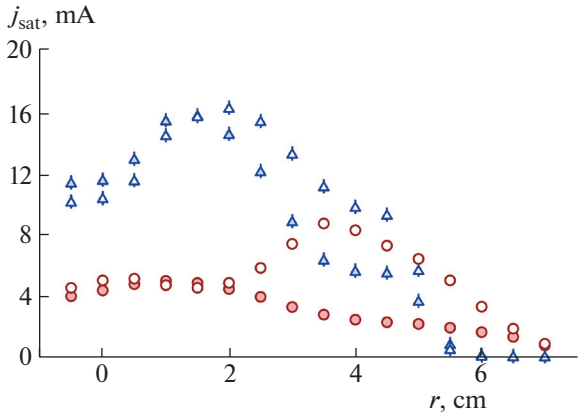

Fig. 13. Radial distributions of ion saturation currents from "upstream" and "downstream" sides (empty and filled symbols, respectively). Blue triangles and red circles correspond to helical and straight fields, respectively.

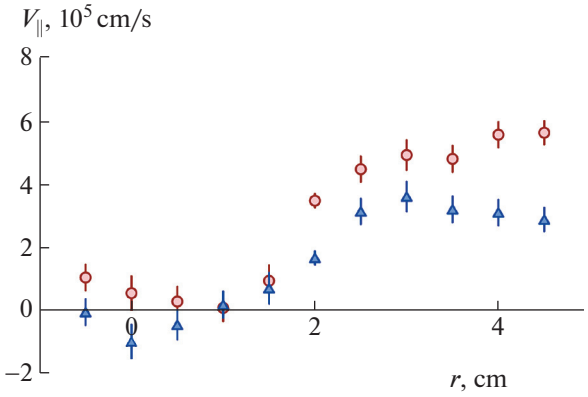

Fig. 14. Radial dependences of longitudinal component of flow velocity at $Z = 2.94$ m. Red circles and blue triangles correspond to straight and helical fields, respectively.

umn was one-third less than the maximum one. With increasing magnetic field corrugation, the maximal density increases and the region of higher plasma density shifts towards the axis (Fig. 5).

Using the data in Fig. 13 and formulas from Section 3, we can calculate the longitudinal velocity of motion. Figure 14 shows the radial dependences of the longitudinal component of the flow velocity at $Z =$ 2.94 m obtained in the straight and helical magnetic fields. In both the straight and helical magnetic fields, the velocity maximum is reached at the plasma edge, being ~5×10^6 and ~3×10^6 cm/s, respectively. In the helical field, the longitudinal velocity is lower than that in the straight field, though it changes its direction at the plasma radius of 1 cm. This indicates the improved plasma confinement in the helical magnetic field and its transport in the reverse direction towards the transport section.

For this experiment, we can calculate the fraction of trapped particles using the model described in the previous section. At plasma parameters corresponding to the "narrow jet regime," the fractions of trapped particles at the plasma edge and plasma axis are 8 and 6%, respectively. The volume of phase space outside the loss cone sufficient for the existence of such a fraction of trapped particles can be achieved at the mirror ratio $R > 1.02$, which corresponds to the radius $r \approx$ 0.8 cm. This radius is comparable to the Larmor radius of ions, due to which the trapped particles forming the reverse flow can exist in the entire plasma volume.

5. CONCLUSIONS

A series of experiments on studying the spatial characteristics of the plasma flow velocity using the Mach probes and the Doppler spectroscopy diagnostics were carried out at the SMOLA open trap with the helical magnetic field. The measurements were performed in different magnetic field configurations. It was shown that the Mach probe-based diagnostics of the flow velocity can be used in open traps under conditions of plasma rotation. It was found out that the longitudinal velocity of the plasma jet depends on the magnetic field corrugation. The maximum velocity reached was ~4×10^6 cm/s, which is half the velocity of sound for the plasma parameters in the SMOLA device.

In the "narrow plasma jet regime" in the helical field, it was demonstrated that there occurs the reverse flow of ions moving from the endplate towards the plasma source. It was ascertained that such an effect will be observed at the fraction of trapped ions of already 4% and the mirror ratio of $R > 1.02$. The reverse flow was observed in the magnetic field configuration, in which the plasma is detached from the inlet and outlet limiters.

In the helical magnetic field, in the transport section, the longitudinal plasma velocity is lower (~10^6 cm/s) than that in the straight field (~5×10^6 cm/s), which demonstrates the efficiency of helical confinement.

FUNDING

The studies of plasma rotation were supported by the Russian Science Foundation (project no. 22-12-00133). The operation of the SMOLA device was supported by the Ministry of Science and Higher Education of the Russian Federation.

CONFLICT OF INTEREST

The authors of this work declare that they have no conflicts of interest.

REFERENCES

1. R. F. Post, Nucl. Fusion **27**, 1579 (1987). https://doi.org/10.1088/0029-5515/27/10/001

2. T. C. Simonen, A. Anikeev, P. Bagryansky, A. Beklemishev, A. Ivanov, A. Lizunov, V. Maximov, V. Prikhodko, and Yu. Tsidulko, J. Fusion Energy **29**, 558 (2010). https://doi.org/10.1007/s10894-010-9342-7

3. D. Endrizzi, J. K. Anderson, M. Brown, J. Egedal, B. Geiger, R. W. Harvey, M. Ialovega, J. Kirch, E. Peterson, Y. V. Petrov, J. Pizzo, T. Qian, K. Sanwalka, O. Schmitz, J. Wallace, et al., J. Plasma Phys. **89**, 975890501 (2023). https://doi.org/10.1017/S0022377823000806

4. T. Imai, M. Ichimura, Y. Nakashima, M. Sakamoto, I. Katanuma, M. Yoshikawa, T. Kariya, M. Hirata, J. Kohagura, R. Minami, T. Numakura, R. Ikezoe, K. Oki, K. Sakamoto, and GAMMA10 group, Fusion Sci. Technol. **63**, 8 (2013). https://doi.org/10.13182/FST13-1T29

5. H. Gota, M. W. Binderbauer, T. Tajima, A. Smirnov, S. Putvinski, M. Tuszewski, S. A. Dettrick, D. K. Gupta, S. Korepanov, R. M. Magee, J. Park, T. Roche, J. A. Romero, E. Trask, X. Yang, et al., Nucl. Fusion **61**, 106039 (2021). https://doi.org/10.1088/1741-4326/ac2521

6. D. Yakovlev, Z. Chen, P. Bagryansky, A. Bragin, I. Kotelnikov, E. Kuzmin, V. Prikhodko, I. Shikhovtsev, P. Usov, Z. Wang, Q. Zeng, L. Dong, K. Zhang, A. Ivanov, and J. Yu, Nucl. Fusion **62**, 076017 (2022). https://doi.org/10.1088/1741-4326/ac5224

7. A. Burdakov, A. Azhannikov, V. Astrelin, A. Beklemishev, V. Burmasov, G. Derevyankin, V. Ivanenko, I. Ivanov, M. Ivantsivsky, I. Kandaurov, V. Konyukhov, I. Kotelnikov, V. Kovenya, T. Kozlinskaya, K. Kuklin, et al., Fusion Sci. Technol. **51**, 106 (2007). https://doi.org/10.13182/FST07-A1327

8. P. A. Bagryansky, A. V. Anikeev, G. G. Denisov, E. D. Gospodchikov, A. A. Ivanov, A. A. Lizunov, Yu. V. Kovalenko, V. I. Malygin, V. V. Maximov, O. A. Korobeinikova, S. V. Murakhtin, E. I. Pinzhenin, V. V. Prokhodko, V. Ya. Savkin, A. G. Shalashov, et al., Nucl. Fusion **55**, 053009 (2015). https://doi.org/10.1088/0029-5515/55/5/053009

9. D. I. Skovorodin, I. S. Chernoshtanov, V. Kh. Amirov, V. T. Astrelin, P. A. Bagryanskii, A. D. Beklemishev, A. V. Burdakov, A. I. Gorbovskii, I. A. Kotel'nikov, E. M. Magommedov, S. V. Polosatkin, V. V. Postupaev, V. V. Prikhod'ko, V. Ya. Savkin, E. I. Soldatkina, et al., Plasma Phys. Rep. **49**, 1039 (2023). https://doi.org/10.1134/S1063780X23600986

10. V. V. Postupaev, V. I. Batkin, A. V. Burdakov, V. S. Burmasov, I. A. Ivanov, K. N. Kuklin, Yu. A. Lykova, N. A. Melnikov, K. I. Mekler, A. V. Nikishin, S. V. Polosatkin, A. F. Rovenskikh, E. N. Sidorov, and D. I. Skovorodin, Nucl. Fusion **62**, 086003 (2022). https://doi.org/10.1088/1741-4326/ac69fa

11. T. D. Akhmetov, V. I. Davydenko, A. A. Ivanov, and S. V. Murakhtin, Plasma Phys. Technol. **5**, 125 (2018). https://doi.org/10.14311/ppt.2018.3.125

12. A. V. Sudnikov, A. D. Beklemishev, V. V. Postupaev, A. V. Burdakov, I. A. Ivanov, N. G. Vasilyeva, K. N. Kuklin, and E. N. Sidorov, Fusion Eng. Des. **122**, 86 (2017). https://doi.org/10.1016/j.fusengdes.2017.09.005

13. V. V. Postupaev, A. V. Sudnikov, A. D. Beklemishev, and I. A. Ivanov, Fusion Eng. Des. **106**, 29 (2016). https://doi.org/10.1016/j.fusengdes.2016.03.029

14. A. D. Beklemishev, Fusion Sci. Technol. **63**, 355 (2013). https://doi.org/10.13182/FST13-A16953

15. A. D. Beklemishev, Phys. Plasmas **22**, 103506 (2015). https://doi.org/10.1063/1.4932075

16. A. D. Beklemishev, AIP Conf. Proc. **1771**, 040006 (2016). https://doi.org/10.1063/1.4964191

17. A. V. Sudnikov, A. D. Beklemishev, V. V. Postupaev, I. A. Ivanov, A. A. Inzhevatkina, V. F. Sklyarov, A. V. Burdakov, K. N. Kuklin, A. F. Rovenskikh, and N. A. Melnikov, Plasma Fusion Res. **14**, 2402023 (2019). https://doi.org/10.1585/pfr.14.2402023

18. A. V. Sudnikov, A. D. Beklemishev, A. A. Inzhevatkina, I. A. Ivanov, V. V. Postupaev, A. V. Burdakov, V. V. Glinskiy, K. N. Kuklin, A. F. Rovenskikh, and V. O. Ustyuzhanin, J. Plasma Phys. **86**, 905860515 (2020). https://doi.org/10.1017/S0022377820001245

19. A. V. Sudnikov, I. A. Ivanov, A. A. Inzhevatkina, M. V. Larichkin, K. A. Lomov, V. V. Postupaev, M. S. Tolkachev, and V. O. Ustyuzhanin, J. Plasma Phys. **88**, 905880102 (2022). https://doi.org/10.1017/S0022377821001276

20. A. V. Burdakov and V. V. Postupaev, Phys.—Usp. **61**, 582 (2018). https://doi.org/10.3367/UFNe.2018.03.038342

21. A. Burdakov, A. Azhannikov, V. Astrelin, A. Beklemishev, V. Burmasov, G. Derevyankin, V. Ivanenko, I. Ivanov, M. Ivantsivskiy, I. Kandaurov, V. Konyukhov, I. Kotelnikov, V. Kovenya, T. Kozlinskaya, K. Kuklin, et al., Fusion Sci. Technol. **51**, 106 (2007). https://doi.org/10.13182/FST07-A1327

22. A. A. Inzhevatkina, A. V. Burdakov, I. A. Ivanov, K. A. Lomov, V. V. Postupaev, A. V. Sudnikov, and V. O. Ustyuzhanin, Plasma Phys. Rep. **47**, 794 (2021). https://doi.org/10.1134/S1063780X21080055

23. I. Ivanov, V. Ustyuzhanin, A. Sudnikov, and A. Inzhevatkina, J. Plasma Phys. **87**, 845870201 (2021). https://doi.org/10.1017/S0022377821000131

24. K.-S. Chung, Plasma Sources Sci. Technol. **21**, 063001 (2012). https://doi.org/10.1088/0963-0252/21/6/063001

25. M. Hudis and L. M. Lidsky, J. Appl. Phys. **41**, 5011 (1970). https://doi.org/10.1063/1.1658578

26. J. J. Gosselin, S. C. Thakur, S. H. Sears, J. S. McKee, E. E. Scime, and G. R. Tynan, Phys. Plasmas **23**, 073519 (2016). https://doi.org/10.1063/1.4954820

Translated by I. Grishina